Nanostructure Formation through β-Sheet Self-Assembly in Silk-Based Materials

Osman Rathore and Dotsevi Y. Sogah*

Department of Chemistry and Chemical Biology, Baker Laboratory, Cornell University, Ithaca, New York 14853-1301

Received September 7, 2000; Revised Manuscript Received December 4, 2000

ABSTRACT: Biomolecular *Bombyx mori* silk-based multiblock copolymers of poly(ethylene oxide)(PEO) and GlyAlaGlyAla prepared by step-growth polymerization based on a modular chemical method have been found to self-assemble into nanostructures. Solid-state ^{13}C NMR, solid-state FTIR, and powder X-ray diffraction provided evidence for the β-sheet self-assembly. The overall β-sheet content was as high as 90%. The building blocks had significant impact on the solid-state structure of the resulting polymer. Longer PEO spacers lowered the tendency to self-assemble into antiparallel β-sheets and implicated the existence of PEO-sequestered isolated β-sheets. Differential scanning calorimetry, transmission electron microscopy, and atomic force microscopy confirmed nanostructure formation and microphase separation. The microphase-separated morphology of the polymers contained 20−50 nm peptide domains dispersed in a continuous PEO phase on which was superimposed a 100−150 nm superstructure due to the polymers' polydispersity and multiblock character. Instron measurements suggested that mechanical properties could be modulated by manipulating the building blocks.

Introduction

Nature has modulated and optimized the properties of biopolymers over many years via exquisite nanostructure engineering. It manipulates primary sequences of polypeptides, and consequently their secondary and tertiary structures, to achieve the desired functions. Fibrous proteins are excellent examples of biopolymers whose molecular architecture is correlated to macroscale attributes. Some of the naturally occurring structural proteins, such as silks, collagen, elastin, amelogenins, and enamelins, derive their properties from repetitive peptide sequences that fold into regular structural elements and impart excellent mechanical properties to the biopolymers.[1] The repetitive nature of their primary sequences is reminiscent of synthetic segmented multiblock copolymers. This realization has inspired our explorations into the use of well-defined secondary structural motifs to control the structure and properties of protein-based synthetic polymers.[2,3]

Biomolecular materials based upon natural silks have received considerable attention due to their outstanding mechanical properties.[1] Silks derive their extraordinary strength from hard, crystalline antiparallel β-sheet structures that form temporary noncovalent cross-links. Their elasticity and toughness have been attributed to amorphous peptide regions that contain bulky side groups and unordered conformations. Several research laboratories have obtained silk analogues via genetic methods,[1c−d,4] while others and we have resorted to a modular chemical approach.[1b,2,3] Whereas the recombinant DNA approach delivers superb control over both sequence and molecular weight, the power of the modular chemical approach lies in the capability it provides for incorporating into synthetic biomolecular materials diverse synthetic and natural segments in a sequence-controlled manner. In exploring the full potential of the chemical modular technique, our goal has not been to completely emulate the properties of the natural materials but rather to develop the fundamental knowledge necessary to rationally vary the architecture of biomolecular materials and thereby tailor their properties to desired functions.

The objective of the work reported here is to take advantage of the tendency of β-sheets to self-assemble into ordered stacks in order to control nanostructure formation in segmented multiblock copolymers. To accomplish this, we have taken a dual-design approach (Chart 1). The first one (Chart 1a) involves the use of an aromatic hairpin turn to nucleate parallel β-sheet formation in the polymer backbone. Our earlier studies demonstrated that preformed secondary structures, including antiparallel and templated parallel β-sheets, incorporated into appropriate building blocks, were retained in the structure of the final polymer both in the solid state and in solution.[2,3] More recently, we provided preliminary evidence for antiparallel self-assembly of phenoxathiin-templated parallel β-sheets in *Bombyx mori* silk-based segmented multiblock copolymers.[2a] The present design incorporates a much longer PEO linker between the peptides to facilitate higher chain mobility and improve processing of the resulting polymers. To permit direct comparison the design retains the parallel β-sheet template.

The second design involves a nontemplated system (Chart 1b) that is fully linear and, thus, free to self-assemble intra- and intermolecularly into either parallel or antiparallel β-sheets. The linkage of the peptides to the PEO segment is identical to the first design in that they are joined in a head-to-head and tail-to-tail fashion. The ability of either the peptide-containing building block or the corresponding polymer to self-assemble into antiparallel β-sheets is not dependent on whether the catenation is tail-to-tail, head-to-head, or head-to-tail.[2a,b,3a,b] This provides flexibility in building block selection and permits choosing the linkage that best lends itself to a more facile step-growth polymerization reaction. The unnatural head-to-head or tail-to-tail linkage is easily amenable to "AA + BB" step-growth polymerization which tolerates a broader monomer scope. In all cases, the peptide segment is the tetrapep-

10.1021/ma001553x CCC: $20.00
Published on Web 02/02/2001

Chart 1

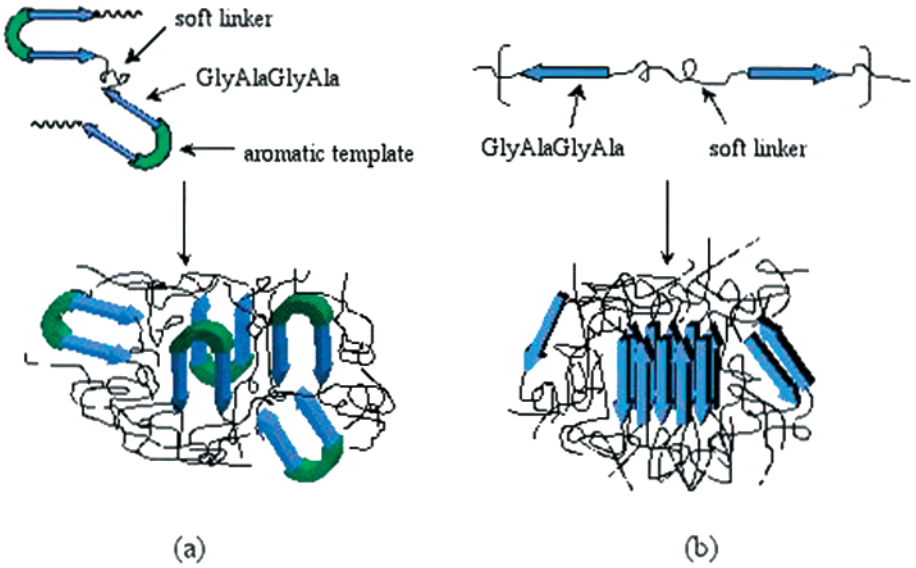

Chart 2

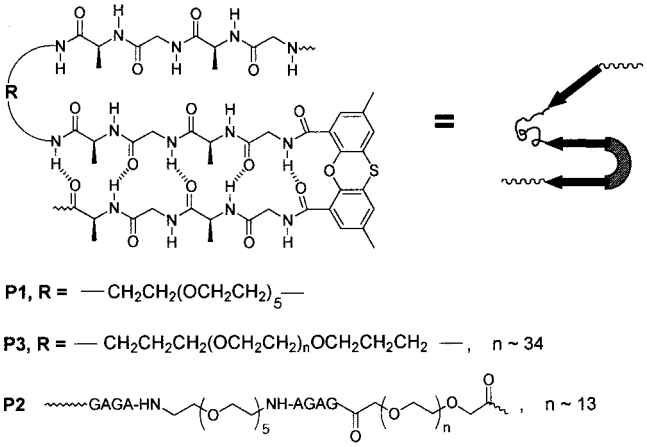

tide GlyAlaGlyAla based on the crystalline domain of *B. mori* silk.

This paper reports the synthesis, physical property measurements, and the detailed study of the relative propensity of **P2** (nontemplated, Chart 2) and **P3** (templated, Chart 2) to self-assemble into nanostructures, and compares their properties to those of the structurally related **P1**[2a] reported previously. A judicious utilization of solid-state ^{13}C NMR, solid-state FTIR, powder X-ray diffraction, transmission electron microscopy, atomic force microscopy, and differential scanning calorimetry reveals that both designs lead to materials that self-assemble into β-sheet nanostructures.

Results and Discussion

Synthesis. The polymers were synthesized utilizing our recently introduced modular chemical approach.[2,3] The preparation of **P2** was effected by catenation of hexakis(ethylene glycol)-based peptidic diamine **2**[2a] with the commercially available poly(ethylene glycol) bis(carboxymethyl) ether (**3**)[5] in solution (DMSO/DPPA/Et_3N) (Scheme 1).[6,7] Dialysis in aqueous solution removed low molecular weight components. Size exclusion chromatography (SEC) of the dialyzed polymer gave a unimodal distribution with M_w = 25 700 and M_n = 16 240 (Table 1). Viscosity measurements in dichloroacetic acid gave an inherent viscosity (η_{inh}) of 0.47 dL·g^{-1}.

The poly(ethylene glycol)-based octapeptide building block (**5**, Scheme 2) needed for the preparation of **P3** was synthesized from the commercially available α,ω-bis(aminopropyl) poly(ethylene glycol) (**4**) and the BOC-protected GlyAlaGlyAla using standard HOBt/DCC coupling techniques and 2,4,6-collidine as catalyst. Aqueous workup followed by dialysis in aqueous solution provided **5** in good yield. ^1H NMR showed the product to be clean and highly disubstituted with NMR-estimated molecular weight of 2800. This was confirmed by SEC which gave a unimodal peak and M_w = 2623, M_n = 2492, and M_w/M_n = 1.05. This material was reacted (Scheme 2) with the aromatic hairpin template (**7**) in a step-growth fashion to yield **P3**.[2a] After purification of the product by dialysis, SEC gave M_w = 13 450 and M_n = 7411 (Table 1).

Evidence for the Presence of β-Sheets in the Solid-State Structure of P2. The extent to which self-assembly into nanostructures occurs is controlled by the β-sheet content. Hence, it was necessary to first establish the presence, type, and amount of β-sheets in the polymers. Evidence for the presence of regular secondary structures in GlyAlaGlyAla-containing polymers and for self-assembly of the peptide domain in solid-state can be obtained from solid-state ^{13}C NMR[2a,9,10] and FTIR.[2a,b,3a,11,12] The former has been used extensively to evaluate β-sheet formation and content in native *B. mori* silk[9] and artificial silk-based segmented block copolymers containing GlyAlaGlyAla tetrapeptide.[2a] Similarly, the amide I carbonyl stretching frequencies in solid-state FTIR of peptides and proteins have been used, not only to establish the presence of β-sheet and other secondary structures in the solid-state[2a,b,3,11,12] but also to distinguish between parallel (pβ) and antiparallel (apβ) β-sheets.[2,3]

Figure 1a shows the solid-state ^{13}C NMR spectrum of **P2**. Overall, the shape and the chemical shifts of both Ala-C$^\alpha$ and Ala-C$^\beta$ peaks are consistent with those observed for *B. mori* silk fibroin and poly(AlaGly) in their silk II form.[9c] Examination of the Ala-C$^\beta$ region of the spectrum (19−24 ppm) reveals a broad resonance at 21 ppm due to Ala residues in aggregated β-sheets.

Scheme 1

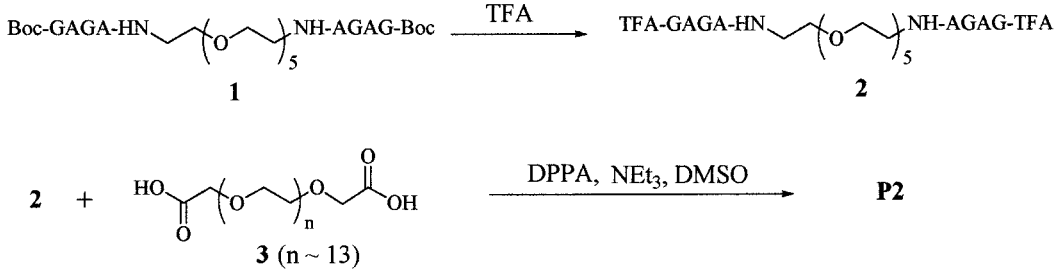

Table 1. Synthesis of Polyamides P2 and P3

polymer	[Mon] (M)	reacn time (h)	yield (%)	M_n(SEC)[a]	M_w(SEC)[a]	M_p(SEC)[b]
P2	0.27	48	82	16 240	25 700	24 280
P3 (soln)	0.14	96	67	7411	13 450	6381
P3 (interfac)	0.02	48	45	8105	18 730	17 370

[a] SEC was performed in DMSO using PEO standards. [b] SEC peak MW.

This is corroborated by the Ala-C$^{\alpha}$ resonance at 49.5 ppm. The absence of any noticeable shoulder downfield (51−52 ppm) to the Ala-C$^{\alpha}$ peak and upfield (15−19 ppm) to Ala-C$^{\beta}$ peak suggests that the structure does not contain a substantial amount of non-β conformations. These results suggest that the solid-state structure of **P2** contains predominantly β-sheet stacks. The total β-sheet content was estimated from the NMR spectrum to be ca. 90% which is substantially higher than that reported for native *B. mori* silk (72%)[10c] and structurally related **P1** (80%).[2a] Hence, in the absence of the aromatic template, the resulting polymer readily assembles into β-sheets.

As solid-state ^{13}C NMR does not necessarily distinguish between parallel and antiparallel β-sheets and provides only the total β-sheet content, the type of β-sheet must be determined using other analytical methods. The evidence for the β-sheet assembly in **P2** being either parallel or antiparallel was obtained from solid-state FTIR and powder X-ray diffraction. The resolution enhanced solid-state FTIR (top, dotted line) spectrum together with the second derivative (bottom, solid line) spectrum of **P2** is shown in Figure 2. The second derivative plot reveals bands at 1630 and 1685 cm^{-1} that are diagnostic for antiparallel β-sheets. There is no evidence for the presence of parallel β-sheets which would have given infrared bands at 1645 cm^{-1}. This finding is significant as it suggests that the natural tendency of the peptide to form antiparallel β-sheets is too strong to be overridden simply by the manner in which the peptides are linked. Hence, even though the linkage in **P2** is head-to-head, tail-to-tail (a parallel linkage) rather than head-to-tail (antiparallel linkage), the polymer forms mainly antiparallel β-sheet structures in the solid state. Consistent with the ^{13}C NMR findings, the FTIR spectrum reveals bands due to random (*r*, 1655 cm^{-1}) and non-β-sheet (non-β, 1663 and 1675 cm^{-1}) conformations that are considerably weaker than the antiparallel β-sheet bands. Furthermore, powder X-ray diffraction of **P2** (Figure 3) shows peaks with *d* spacings of 4.63, 4.26, 3.74, and 2.93 Å that are in complete agreement with the antiparallel β-sheet *d* spacings reported for $(AlaGly)_n$ by Fraser et al.[13] and Tirrell et al.[14] Therefore, the solid-state FTIR and X-ray results provide conclusive evidence that **P2** self-assembles into predominantly antiparallel β-sheets (Chart 1b).

Evidence for the Presence of β-Sheets in the Solid-State Structure of P3. The solid-state ^{13}C NMR spectrum of **P3** is shown in Figure 1b. Similar to what was previously observed for polymers containing Gly-AlaGlyAla β-sheets templated by phenoxathiin,[2a] the resonance of the methyl groups on the aromatic unit (ca. 20 ppm) overlapped that of the Ala-C$^{\beta}$ (ca. 21 ppm), which limits accurate utilization of this resonance. The presence of β-sheets in **P3** is, however, evident from the 49.5 ppm (shoulder) resonance. Surprisingly, the spectrum is dominated by peaks due to non-β conformations as evidenced by the presence of a much larger peak at 51 ppm and a shoulder at 19 ppm. Consequently, the fraction of the Ala residues present in β-sheet stacks estimated from the ^{13}C NMR spectrum is ca. 30%, which is considerably less than that obtained for **P1** (80%). This is unexpected since the two polymers differ only in the length of the PEO linker. The longer PEO in **P3** was expected to impart higher chain mobility and hence facilitate aggregation of the β-sheets into well-defined domains.

To shed more light on the ^{13}C NMR results, solid-state FTIR studies were performed on **P3**. The spectrum in Figure 4 shows bands at 1645 (sharp) and 1636 cm^{-1} corresponding to parallel β-sheets. This clearly confirms that the aromatic reverse-turn mimic templates intrastrand hydrogen bonding in the expected parallel fashion.[2b] Self-assembly of these parallel β-sheets into antiparallel stacks is indicated by the presence of bands at 1636 (overlapping the parallel β-band) and 1699 cm^{-1}. The solid-state FTIR spectrum shows the presence of substantial amounts of random and non-β conformations, thus confirming the solid-state ^{13}C NMR results that also indicate an increase in non-β relative to β-sheet conformations. Because the major difference between **P1** and **P3** is in the length of the linkers, it can be inferred from the results that increasing the number of the oxyethylene units from 6 to about 34 leads to an unexpected considerable reduction in the total β-sheet content and concomitant increase in non-β structures.

Further evidence for the spacer length being the major contributing factor was obtained from FTIR studies of the building block **5**. Perusal of its solid-state FTIR spectrum shown in Figure 5 revealed antiparallel β-sheets (1629 and 1685 cm^{-1}), a significant contribution from random (1654 cm^{-1}) and non-β (1670 cm^{-1}) conformations, and no indication of parallel β-sheet formation. Hence, as observed for building block **1**,[2a] a parallel oligopeptide linkage is not sufficient to induce parallel β-sheet formation. This is in agreement with our earlier studies that showed that formation of parallel β-sheets

Scheme 2

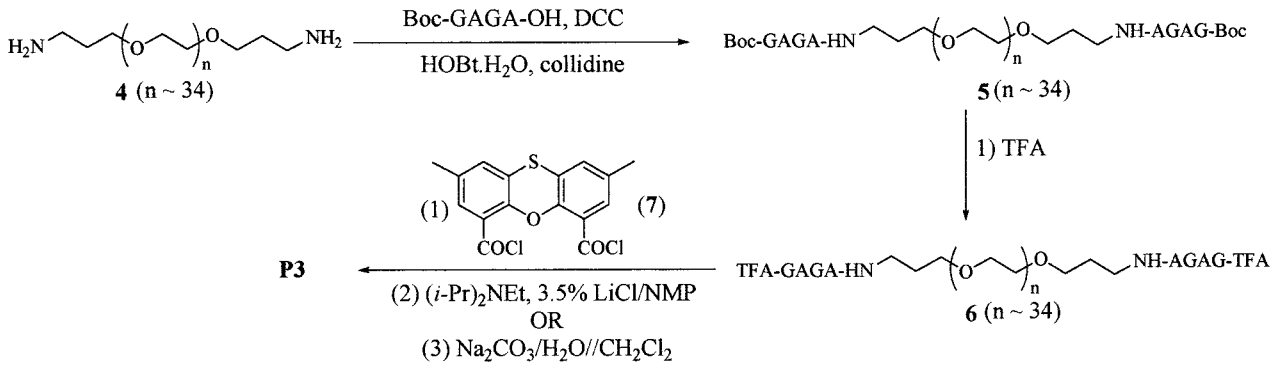

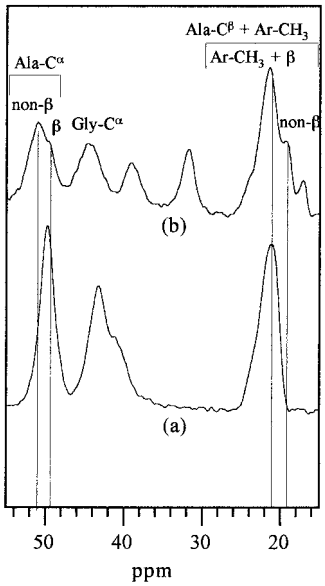

Figure 1. Ala-C^{α} and Ala-$C^{\beta}H_3$ peak region from the solid-state ^{13}C NMR spectra of (a) **P2** and (b) **P3**.

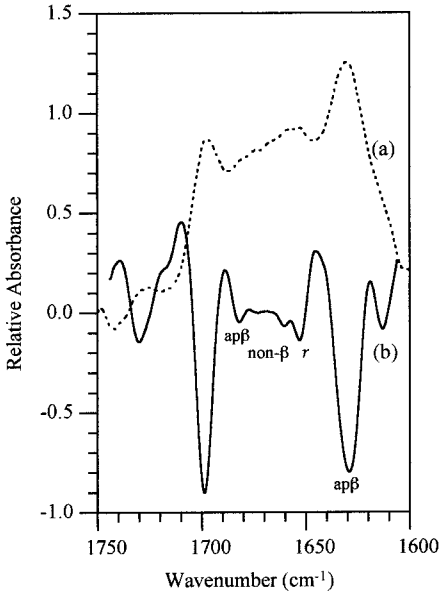

Figure 2. Solid-state FTIR of **P2** (KBr, 2.0 cm^{-1} resolution, room temperature): (a) resolution-enhanced; (b) second derivative. [Key: apβ, antiparallel β-sheet; *r*, random coil; non-β, non-β-sheet conformations.]

through intramolecular hydrogen bonding in systems where flexible linear linkers replaced the rigid template was entropically prohibited.[2b]

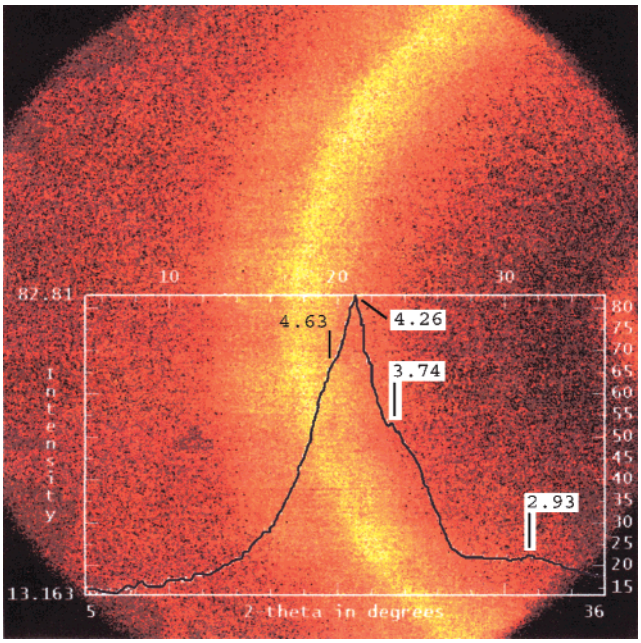

Figure 3. Solid-state FTIR of **5** (KBr, 2.0 cm^{-1} resolution, room temperature): (a) resolution-enhanced; (b) second derivative. [Key: apβ, antiparallel β-sheet; *r*, random coil; non-β, non-β-sheet conformations.]

The presence of a substantial amount of non-β conformations in Figure 5 contrasts the results for **1** whose solid-state FTIR spectrum showed a predominant formation of antiparallel β-sheets but a much lower non-β conformation content.[2a] These results suggest that increasing the length of the linker is, indeed, responsible for the differences in the behavior of the building blocks. Therefore, the increased tendency for **P3** to predominantly form non-β structures is a manifestation of a similar tendency in its peptide building block.

The nature of the non-β structures is not obvious. We hypothesize that hydrogen bonding to the large amount of PEO present reduces the extent of β-sheet formation in a manner analogous to using a polar solvent to disrupt inter- and intrastrand hydrogen bonding, especially at low peptide concentrations. The GlyAlaGlyAla segments that could not readily come together to form β-sheets might become isolated and buried in the PEO domain, possibly hydrogen bonded to the PEO oxygen atoms. These might appear as non-β structures leading to the lower observed overall antiparallel β-sheet content in **5**. A similar behavior in **P3** would result in isolation of the templated parallel β-sheet domains in the PEO matrix which would reduce their tendency to self-assemble in an antiparallel fashion. Literature

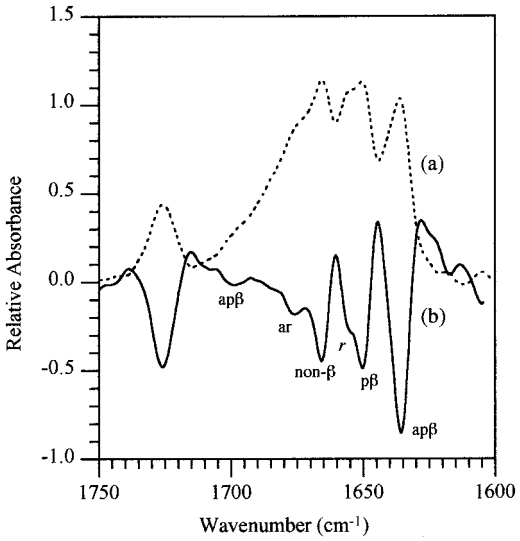

Figure 4. Solid-state FTIR of **P3** (KBr, 2.0 cm^{-1} resolution, room temperature): (a) resolution-enhanced; (b) second derivative. [Key: apβ, antiparallel β-sheet; pβ, parallel β-sheet; *r*, random coil; non-β, non-β-sheet conformations.]

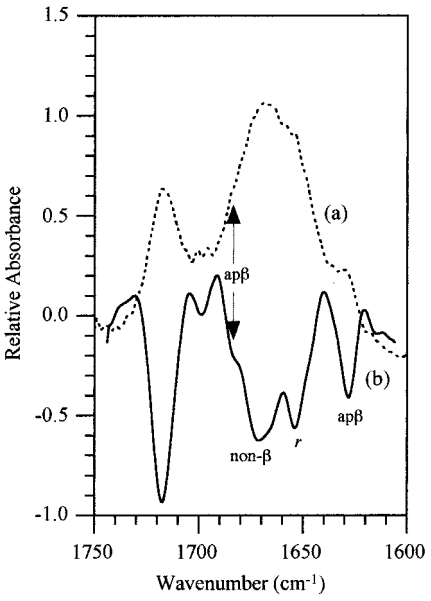

Figure 5. Powder X-ray diffraction spectrum of polymer **P2**.

values for solid-state ^{13}C NMR chemical shifts are principally for aggregated β-sheets. Therefore, solid-state ^{13}C NMR could underestimate the total β-sheet content in **P3**, especially if the isolated parallel β-sheets do not have the same chemical shifts as aggregated antiparallel β-sheets. This isolation of the templated parallel β-sheets in the PEO matrix is consistent with the enhanced intensity (the highest ever observed) for the 1645 cm^{-1} parallel β-band and the reduced antiparallel β-band.

Consistent with the above deductions from the spectroscopic data, the powder X-ray diffraction pattern for **P3** (Figure 6) shows sharp peaks at 4.68 and 3.89 Å. Such relatively sharp features in the powder diffraction pattern have only been observed previously for unimolecular models of the phenoxathiin-templated parallel β-sheet structures that gave strong peaks at *d* spacings of 4.65 and 4.17 Å.[2b] Hence, the *d* spacings observed for **P3** are due to the templated parallel β-sheets, which further supports the hypothesis that the long PEO linker is serving to "dilute" the templated parallel

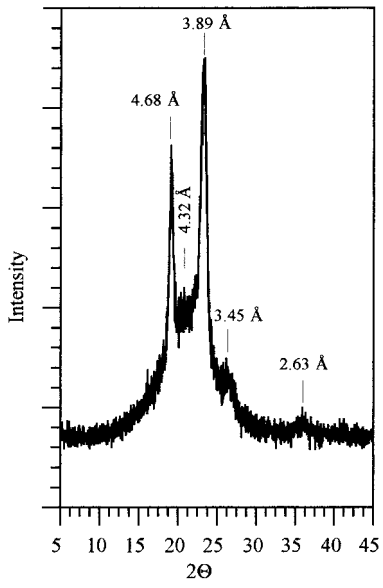

Figure 6. Powder X-ray diffraction spectrum of polymer **P3**.

Table 2. Thermal Properties of 5 and Solution Polymerized Polyamides P1−P3[a]

polymer	T_g (°C) (DSC)	T_m (°C) (DSC)	$T_{d,onset}$ (°C) (TGA)
silk fibroin[b]	175		250
poly(AlaGly)[c]			293
P1[d]	−57, 111	*e*	312
P2	−57, 0	116	300
P3	−98, −50	9	184 (5% loss) 284 (82% loss)

[a] Performed under nitrogen atmosphere. [b] Silk fibroin in random coil conformation; taken from Nakamura, S.; Magoshi, J.; Magoshi, Y. In ref 1d, pp 211−221. DSC heating rate: 8 °C/min. [c] Reference 3c. [d] Reference 2a. DSC heating rate: 10 °C/min. [e] None observed.

β-sheets. In effect, the observed diffraction pattern might be regarded as that of several unimolecular models of templated parallel β-sheets which, owing to the very long PEO linker, behave independent of each other.

The ^{13}C NMR, FTIR, and X-ray diffraction analyses provide conclusive evidence for the existence of parallel β-sheets nucleated by the phenoxathiin template in **P3**. Because of its relatively longer PEO spacers, the polymer shows less tendency to self-assemble in an antiparallel fashion unlike the previously studied **P1** (Chart 1a). To our knowledge, the results represent the first clear observation of isolated parallel β-sheets in the solid-state structure of a biopolymer. The behavior of both **P3** and the previously studied **P1** in the solid state has now been traced to that of their respective building blocks. The results point to the importance of controlling the structure of the building block as it has significant impact on the structure of the resulting polymer.

Evidence for Microphase Separation in P2 and P3. As expected from its segmented structure, **P2** exhibited multiple transitions in differential scanning calorimetry (DSC) measurements: a T_m at 115.6 °C and two glass transition temperatures (T_g's) at −57.2 and +0.4 °C (Table 2) with no T_m for a crystalline PEO domain. The distinct T_m was assigned to self-assembled polypeptide domain, the lower T_g to the polyether-rich phase and the second T_g to the peptide-rich domain. However, a T_g of 0.4 °C is low for pure polypeptide domains.[15] It is likely that the polypeptide domains are

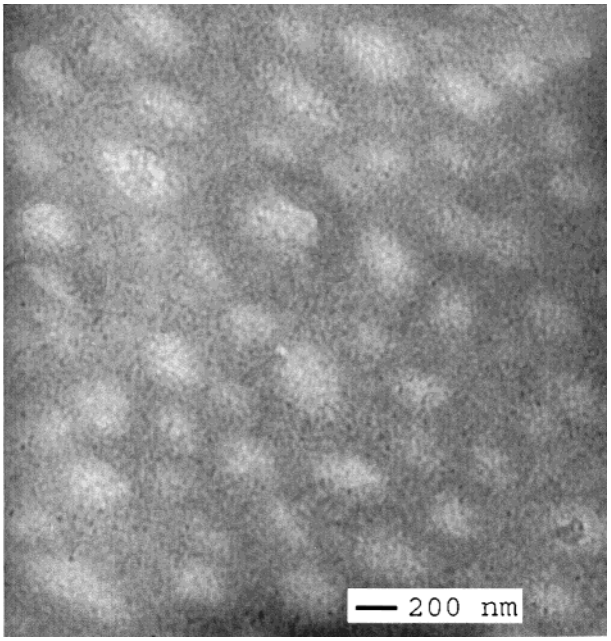

Figure 7. TEM image of a solvent-cast thin film of **P2**.

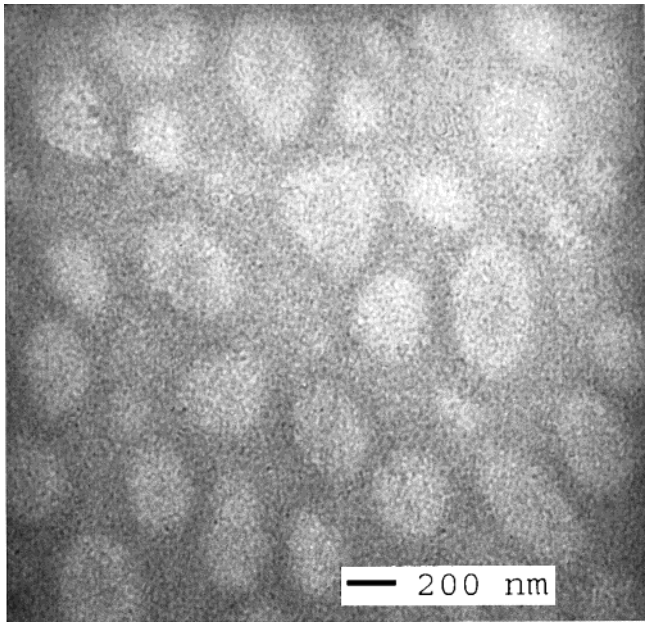

Figure 8. TEM image of a solvent-cast thin film of **P3**.

interpenetrated to some extent by the polyether segments leading to some mixing of phases and consequent lowering of the T_g. The suggested interpenetrating morphology has been seen previously for **P1** and confirmed here for **P2** and **P3** by TEM and AFM (vide supra).

P3 also exhibited three thermal transitions: a T_m at 9 °C and two T_g's at −98 °C and −50 °C. The T_m was attributed to PEO-rich domains consistent with the PEO linker being longer and therefore able to crystallize below room temperature. The lower T_g was due to PEO-rich domains (lit.[15] −115 to −40 °C) while the higher T_g was presumed to be associated with the peptide-rich domains. We have previously reported that increasing the flexibility of the soft segment led to a lower T_g for the resulting peptide-hybrid polymer. Since **P3** contained a long flexible PEO linker, it is not unreasonable for its T_g to be considerably lower than the values of 111−186 °C observed for the far more rigid systems previously investigated.[2a,b] The results for **P3** are therefore in agreement with the trend observed for this series of silk-based polymers containing phenoxathiin-templated parallel β-sheets.[2a,b] The relatively lower T_g associated with the polypeptide-phase in **P3** again suggests a mixing of phases.

The Morphology of Nanostructures of P2 and P3 As Revealed by Transmission Electron Microscopy (TEM) and Atomic Force Microscopy (AFM). Figures 7 and 8 show the TEM images obtained for **P2** and **P3**, respectively, from TFE solution-cast films stained with RuO_4. The figures reveal phase-separated morphologies with pale islands of a polypeptide-rich phase (20−50 nm) dispersed in a darker continuous polyether-rich matrix. The larger domains ("superstructures"), on the order of 100−150 nm, consisted of agglomerations of smaller peptide particles with the polyether dispersed between them. Chung et al. have observed a similar morphology for nylon-6-based block copoly(ether amides).[16]

The issue arises as to what phenomenon is responsible for the superstructures overlaying the ordinary microdomain separation. We believe this is due to the polydisperse and multiblock nature of the polymers. Despite a fair amount of work done in modeling and studying phase separation in block copolymers, the phenomenon of phase separation in polydisperse multiblock copolymers is relatively poorly understood.[17,18] Most of the models are difficult to apply especially to cases where there is some degree of interphase penetration as is expected to be the case for **P2** and **P3** based upon the morphology seen for **P1**.[2a] However, a model constructed by Semenov for polydisperse multiblock copolymers did, indeed, predict the existence of superstructures.[19] Semenov suggested that randomness in block lengths could result in structures with two levels of organization: a microphase separation between regions with different block molecular weights (superstructures) superimposed on an ordinary microdomain separation. Because **P2** and **P3** were made by step-growth polymerization they are polydisperse (M_w/M_n = 1.58−1.81) although the polyether-containing building blocks either have low polydispersity (M_w/M_n = 1.05 for **5**) or are unimolecular ($M_w = M_n$ for **2**). Therefore, it is not surprising that these polymers exhibit phase-separated morphology that qualitatively fits the Semenov model. The 100−150 nm polypeptide-rich domains are presumed to comprise of chains that have the highest polypeptide/polyether ratio. This ratio would be highest for chains containing the shortest polyether blocks and having polypeptides as end segments.

The mixing of phases and the formation of superstructures are more clearly revealed in the AFM images of **P2** and **P3** (Figures 9 and 10). Stiffer regions correspond to hard polypeptide domains and therefore appear higher (lightest color).[20] This is seen more clearly in the contour plots (Figure 9b). Besides the ca. 100−150 nm islands of polypeptide phase (corresponding to the 100−150 nm polypeptide domains in the TEM images), the morphology has a mottled appearance that is consistent with the overall interpenetrating morphology observed in the TEM and implicated by the DSC studies.

Film Formation and Mechanical Properties. To determine the extent to which the observed morphology manifests itself in the mechanical properties of the polymers, stress−strain curves were obtained on films

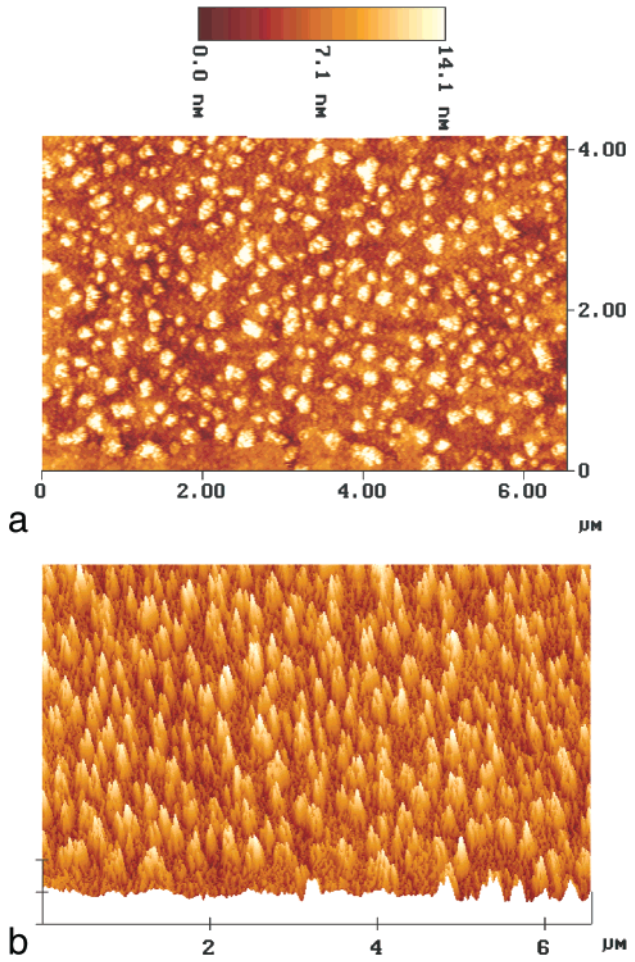

Figure 9. Tapping mode AFM image of **P2** spin-coated on silicon wafer: (a) topographical plot; (b) contour plot.

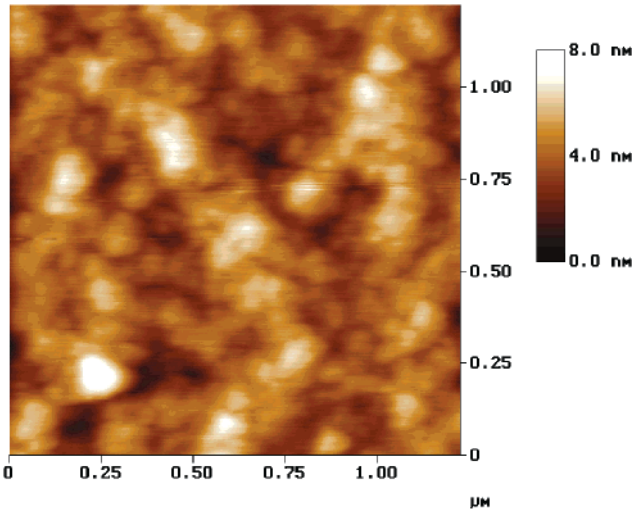

Figure 10. Tapping mode AFM image of **P3** spin-coated on silicon wafer.

of **P2** and **P3**. **P2** was cast as clear colorless films onto glass slides from 50% (w/v) solutions in TFE using a micrometer film applicator. The films were dried in air, peeled off, and then dried in vacuo overnight at 60 °C prior to testing. The results are summarized in Table 3. Each entry for **P2** is an average of three to five measurements. Representative stress−strain curves for **P2** films are presented in Figure 11. Clearly, faster loading rates gave higher elongation and better tensile strength for films sheared at the same rate (Figure 11, part b vs part c). At the same loading rate, lower shear rates resulted in slightly worse tensile properties ((Figure 11, part a vs part b). It can be seen from the results in Table 3 that replacement of the rigid aromatic template of **P1**[2a] with the flexible oligo(ethylene glycol) chain (**P2**) resulted in a tougher and stronger material. The observed tensile modulus and tensile strength are about a factor of 10 lower than those of either molded nylon-6,6 or nylon-6.[21] To our knowledge, there are no published data on mechanical properties of films of silk materials. All available data are for oriented fibers which prevents direct comparison. Efforts are in progress to obtain high quality fibers from **P2**.

Table 3. Mechanical Properties of P2 and P3[a]

polymer	shear rate ($cm \cdot s^{-1}$)	loading rate (s^{-1})	modulus (MPa)	tensile strength (MPa)	elongation at break (%)
P2	30−60	0.03%	249 ± 50	7.5 ± 1.1	8.4 ± 1.6
P2	30−60	0.50%	210 ± 9	14.0 ± 0.4	21.2 ± 6.0
P2	6	0.03%	131 ± 43	3.4 ± 0.7	13.5 ± 1.3
P3	*b*	0.03%	12	0.62	5.9

[a] Entries for **P2** are averages of three to five measurements; entries for **P3** are for a representative measurement. [b] **P3** films were obtained from a mold.

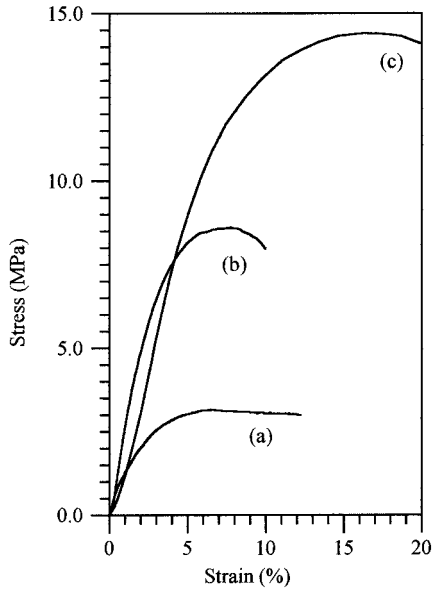

Figure 11. Stress−strain measurements on **P2** films: (a) shear rate, 6 $cm \cdot s^{-1}$; rate of extension, 0.03% s^{-1}; (b) shear rate, 30−60 $cm \cdot s^{-1}$; loading rate, 0.03% s^{-1}; (c) shear rate, 30−60 $cm \cdot s^{-1}$; loading rate: 0.5% s^{-1}.

Good films could not be consistently obtained for **P3** using the same film applicator in that the film could not be easily peeled off without breaking. Use of a nonsolvent, such as diethyl ether, to float the films off the glass substrate gave films with poorer results and highly variable tensile properties. Somewhat better films were obtained by pouring 30% (w/v) TFE solutions into an appropriate mold. After allowing the solvent to evaporate at ambient conditions, the films were removed and dried in vacuo at 70 °C. Figure 12 shows a representative stress−strain curve obtained for such a film. As can be seen from Table 3, the mechanical properties are inferior to those obtained above for **P2**.

Nevertheless, the results for **P2** and **P3** represent a significant improvement in properties. They indicate that the mechanical properties of peptide-hybrid mate-

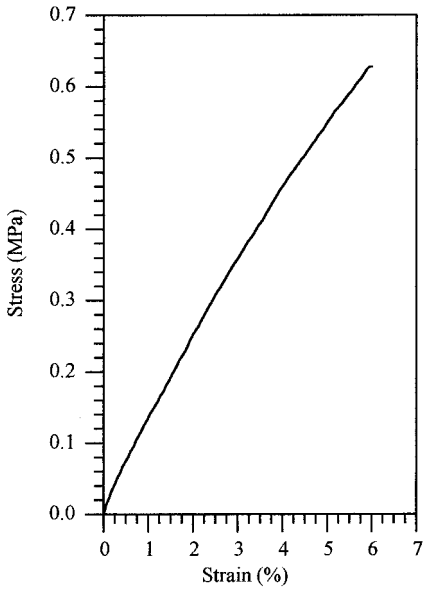

Figure 12. Stress−strain measurement on **P3** film.

rials can be modulated by varying either the nature of the building blocks or the volume fraction of the β-sheet/flexible building block or both. Thus, increasing the length of the linker led to enhancement of toughness comparable to that reported for silk fibers[1d] as evidenced by a higher percent elongation at break. Substituting a flexible diacid for the rigid template but leaving the linker unchanged resulted in further enhancement of tensile properties. Hence, while the amorphous content of the peptide-hybrid polymer seems crucial for toughness control, clearly effective temporary noncovalent cross-links formed by the self-assembled antiparallel β-sheets greatly impact the strength and toughness of the material.

Summary and Conclusions

Two novel polymers, **P2** and **P3**, containing alternating PEO and GlyAlaGlyAla tetrapeptide segments have been prepared and shown to form nanostructures through β-sheet self-assembly. **P2** exhibits solid-state properties very similar to *B. mori* silk fibroin and $(AG)_n$ in their silk II form. A judicious combination of solid-state ^{13}C NMR, solid-state FTIR, and X-ray diffraction analyses provides conclusive evidence for β-sheet self-assembly in **P2** and confirms the existence of parallel β-sheets nucleated by the phenoxathiin template in **P3**. Because of their relatively longer PEO spacers, **P3** and the corresponding building block **5** show a lower tendency to self-assemble in an antiparallel fashion. The results suggest the possible existence of PEO-sequestered isolated parallel β-sheets in **P3**. The behavior of both **P3** and that of the previously studied **P1** in the solid state are traced to those of their respective building blocks, which points to the importance of controlling the structure of building blocks as they have profound impact on at least the solid-state structure of the resulting polymers.

Phase separation and nanostructure formation have been confirmed by DSC, TEM, and AFM. The polymers have morphology in which the peptide domain, estimated to be ca. 10−50 nm, is dispersed in the continuous polyether phase. In addition to the microdomain separation, a secondary level of organization of the polypeptide domains (ca. 100−150 nm) due to aggregation of chains with a high polypeptide/polyether volume fraction has been observed. Instron measurements suggest that the mechanical properties of these novel segmented oligopeptide-containing polymers can be modulated by varying the building blocks. Extending the concept to other soft linkers and polypeptide domains could lead to novel materials with applications as protein/cell immobilization substrates, semipermeable membranes, and medical reconstruction materials.

Experimental Details

Materials. Abbreviations: Ala, alanine; Bn, benzyl; BOC, *N*-*tert*-butoxycarbonyl; DMF, *N*,*N*-dimethylformamide; DMSO, dimethyl sulfoxide; DCC, dicyclohexylcarbodiimide; DMAP, *N*,*N*-dimethylaminopyridine; DPPA, diphenylphosphoryl azide; EtOAc, ethyl acetate; Gly, glycine; HOBt, 1-hydroxybenzotriazole monohydrate; MeOH, methanol; MWCO, molecular weight cutoff; NMP, *N*-methylpyrrolidinone; PEO, poly(ethylene glycol); TFA, trifluoroacetic acid; TFE, trifluoroethanol. Common reagents were purchased from Aldrich, Sigma, or Acros and solvents from Fisher Scientific or Mallinckrodt. Diisopropylethylamine was distilled from ninhydrin and then from CaH_2 onto 4 Å molecular sieves and stored in a drybox. NMP was distilled from CaH_2 onto 4 Å molecular sieves and stored in a drybox. Triethylamine was distilled from P_2O_5. DMSO was distilled from CaH_2 onto 4 Å molecular sieves. Glassware was dried in an oven and cooled under nitrogen where appropriate. Synthesis of 2,8-dimethylphenoxathiin-4,6-dicarbonyl chloride (**7**), and 3,6,9,12,15-pentaoxaheptadecane-1,17-diamido-bis[L-alanylglycyl-L-alanyl(*N*-*tert*-butoxycarbonyl)glycine] (**1**) were performed in accordance with literature procedures.[2a,b] Poly(ethylene glycol) bis(carboxymethyl) ether (**3**, $M_n \sim 600$) and bis-aminopropyl poly(ethylene glycol) (**4**, $M_n \sim 1630$) were purchased from Aldrich and used without purification. Dialyses were performed using Spectra/Por cellulose ester membrane tubing in a continuous exchange water bath at room temperature. Glass slides used as substrates for solvent-cast films were sprayed prior to use with Fluoroglide antistick agent and buffed to improve lubricity.

Characterization. ^1H and ^{13}C NMR spectra were recorded on INOVA-400 or VXR-400S spectrophotometers. FTIR spectra were recorded on a Perkin-Elmer 16PC FTIR spectrometer. Solid-state FTIR samples were prepared as 0.3−0.5 wt % in KBr pellets, and the spectra were obtained with 50 scans at a resolution of 2.0 cm^{-1} for 1750−1600 and 4.0 cm^{-1} from 4000 to 1000 cm^{-1}. Solubility tests of the polymers were carried out at 1 mg/mL concentration. SEC was carried out with a Waters 510 HPLC pump with a Viscotek refractometer/viscometer using a bank of PLgel mixed bed C (5 μm beads) columns. DMSO was used as the eluant at 75 °C and at a flow rate of 0.5 mL/min. The chromatograph was calibrated using monodisperse PEO standards. Inherent viscosity measurements were conducted in dichloroacetic acid solutions at a concentration of 0.55 g/dL with a Cannon Ubbeholde C1 C886 viscometer thermostated at 25 ± 0.1 °C. Thermogravimetric analysis (TGA) and differential scanning calorimetry (DSC) were performed on a Seiko 5200 thermal analysis system with TGA/DTA 220 and DSC 220C units under a positive flow of nitrogen at heating rates of 20 and 10 °C/min, respectively. Glass transition temperatures (T_g's) and melt transitions (T_m's) were recorded from the second heating cycle. Melting points were measured on an Electrothermal IA90 melting point apparatus and are uncorrected. Optical rotations were measured at 25 °C on a Perkin-Elmer 241 polarimeter. Powder X-ray diffraction data for **P2** were obtained on a Bruker-Axs D8 system (λ = 1.5405 Å) with a 2-D detector at 40 kV and 40 mA and for **P3** a $\theta-\theta$ Scintag diffractometer with a Cu source (λ = 1.5405 Å). Solid-state ^{13}C NMR CPMAS spectra were recorded at 75.22 MHz on a home-built instrument. TEM was performed on a JEOL 1200EX using a 120 keV acceleration voltage. TEM samples were prepared by spotting carbon film-coated 300-mesh copper grids with a 1 wt % polymer solution in TFE. The samples were then dried for 4 h at 50 °C in vacuo. The

staining was performed by preparing a fresh RuO_4 solution according to literature procedures.[22] The dried samples were exposed to the RuO_4 solution. Good contrast was achieved for an exposure time of 30 min. Tensile measurements were performed on rectangular films using an Instron tensile testing system (series 1122) at 21 °C and 65% relative humidity. The ends of the films were glued using a 5-min epoxy onto pieces of cardboard that were then clamped during measurements. AFM samples were prepared by spin-coating silicon wafers with a 10% (w/v) solution of the polymer at 4000 rpm and immediately drying the wafer at 115 °C for 1 min in vacuo. The samples were visualized on a Nanoscope III (Digital Instruments), using a 12 μm D scanner in air, in the tapping mode. The AFM was mounted on a homemade antivibration table and on an isolation chamber. AFM tips from Digital Instruments with force constants of 50 N/m (manufacturer's specifications) were employed. A resonant frequency of 300 kHz was used.

Poly(ethylene glycol)-α,ω-di(3-amidopropyl)bis[L-alanylglycyl-L-alanylglycyl(*N-tert*-butoxycarbonyl)glycine] (5). To a 100 mL round-bottom flask equipped with a stirring bar were added BOC−GlyAlaGlyAla−OH (3.30 g, 8.83 mmol), HOBt (1.35 g, 8.83 mmol), and 50 mL of 20% DMF in CH_2Cl_2. The solution was cooled to 0 °C, and 2,4,6-collidine (1.1 mL, 8.82 mmol) was added followed after 10 min by DCC (1.82 g, 8.83 mmol). After stirring for additional 15 min a solution of **4** (1.10 g, 3.91 mmol) in 25 mL of 20% DMF in CH_2Cl_2 was added to the reaction mixture. The cooling bath was removed and the mixture was allowed to stir at room temperature under nitrogen atmosphere for 3 days. The reaction mixture was evaporated and the resulting residue taken up in 100 mL of diethyl ether and filtered. The solids thus obtained were dissolved in CH_2Cl_2 and filtered. The filtrate was extracted successively with 5% citric acid (3 × 125 mL), 5% $NaHCO_3$ (3 × 125 mL), and water (1 × 100 mL), dried over $MgSO_4$, filtered, and evaporated. The resulting residue was dissolved in 60 mL of water and filtered. The filtrate was dialyzed (MWCO 500 Da) for 6 days in a continuous flow water bath. The resulting solution was lyophilized to give a pale yellow foam (**5**) (3.36 g, 39%). Mp: 140−145 °C (broad). $[\alpha]_D25 = -4.0°$ ($c = 1$, DMSO). ^{1}H NMR (400 MHz, ppm, DMSO-d_6): δ 8.17 (t, 2H, Gly-N*H*), 8.02 (d, 2H, Ala-N*H*), 7.84 (d, 2H, Ala-N*H*), 7.75 (t,2H, Gly-N*H*), 6.92 (t, 2H, BOC−N*H*−Gly), 4.20 (collapsed dq, 4H, Ala-α*H*), 3.68 (m, 4H, Gly-α*H*), 3.55 (m, 4H, Gly-α*H*), 3.50 (m, 178H, $-OCH_2CH_2-$), 3.37 (t, 4H, $-OCH_2CH_2CH_2NH-$), 3.07 (collapsed dq, 4H, $-OCH_2CH_2CH_2NH-$), 1.61 (p, 4H, $-OCH_2CH_2CH_2NH-$), 1.36 (s, 18H, BOC−CH_3), 1.20 (d, 6H, Ala-βH), 1.17 (d, 6H, Ala-βH).^{13}C NMR (100 MHz, ppm, DMSO-d_6): 172.64, 171.82, 169.29, 168.20, 155.79, 78.05, 72.33, 69.77, 69.52, 67.93, 60.20, 48.43, 48.19, 43.12, 42.05, 35.81, 29.22, 28.14, 18.27, 17.99. $M_n = 2800$ (by ^{1}H NMR), $M_n = 2853 \pm 41$ (by elemental analysis). SEC (DMSO, PEO standard): $M_n = 2492$, $M_w = 2{,}623$, $M_p = 2687$ (100%). DSC: T_{g1} −112 °C, T_{g2} −50 °C; T_{m1} 5 °C, T_{m2} 127 °C.

Synthesis of P2 in Solution. To a dried 50 mL round-bottom flask equipped with a magnetic stirring bar and a gas-inlet adapter were added **1** (3.20 g, 3.22 mmol) and anhydrous TFA (10 mL) under Ar. The mixture was allowed to stir for 1.5 h and then evaporated. The residual oil was further dried in vacuo at 80 °C. The TFA salt (**2**) was dissolved in 6 mL of DMSO. To the stirred solution was added **3** (2.25 g, 3.22 mmol) as a solution in 6 mL of DMSO. The flask was cooled to ∼5 °C and NEt_3 (4.2 mL, 30.1 mmol) and DPPA (5.0 mL, 23.2 mmol) were added. The reaction was stirred rapidly at 5−8 °C for 30 min and then allowed to warm to room temperature. After 2 days the polymerization mixture was pipetted into 300 mL of EtOAc. The crude product was filtered, dissolved in water and dialyzed for 3 days (MWCO 2000 Da). The polymer was isolated after lyophilization as a pale yellow foam (**P2**) (3.85 g, 82%). DSC: T_{g1} −57 °C, T_{g2} 0.4 °C; T_m 116 °C. TGA: $T_{d,onset}$ 300 °C. $[\alpha]_D^{25} = -8.6°$ ($c = 1.2$, DMSO). SEC: $M_n = 16\,240$; $M_w = 25\,700$; $M_p = 24\,280$. Viscosity (dichloroacetic acid): $\eta_{inh} = 0.48$ dL·g^{-1}. IR (KBr, 4.0 cm^{-1}): 3434 (sh), 3289, 3083, 2944 (sh), 2865, 1734, 1718, 1699, 1685, 1675, 1663, 1655, 1630, 1538, 1448, 1403, 1349, 1290, 1245, 1142 (sh), 1107.

Synthesis of P3 in Solution. The polymerization was performed according to a literature procedure[2a,b] using **5** (1.50 g, 0.53 mmol), anhydrous TFA (4.50 mL), **7** (0.19 g, 0.53 mmol), diisopropylethylamine (1.3 mL, 7.5 mmol), and 3.7 mL of 3.5% LiCl in NMP. The polymerization mixture was allowed to stir in the drybox at ambient temperature for 4 days. The mixture was taken out of the drybox and evaporated under high vacuum. The residue was dissolved in water and dialyzed for 3 days (MWCO 2000 Da). The resulting solution was lyophilized to yield **P3** as a pale yellow solid (1.03 g, 67%). DSC: T_{g1} −98 °C, T_{g2} -50 °C; T_m 9 °C. TGA: $T_{d,onset}$ (dual-stage) 184 °C (5% loss); 284 °C (82% loss). SEC: $M_n = 7411$; $M_w = 13\,450$; $M_p = 6381$. IR (KBr, 4.0 cm^{-1}): 3368 (sh), 3295, 3079, 3069, 2920 (sh), 2870, 1726, 1699, 1685 (sh), 1676, 1666, 1655, 1650, 1636, 1548, 1530 (sh), 1456, 1435 (sh), 1351, 1301, 1287, 1251, 1214, 1144 (sh), 1105.

Synthesis of P3 by Interfacial Polymerization. The polymerization was performed according to a literature procedure[2a,b] using **5** (1.21 g, 0.53 mmol), anhydrous TFA (3.60 mL), **7** (0.15 g, 0.53 mmol), Na_2CO_3 (1.35 g, 12.7 mmol), 11 mL of distilled water, and 11 mL of CH_2Cl_2. The polymer was isolated by evaporating the CH_2Cl_2 after 2 days of rapid stirring and dissolving the solids using additional 50 mL of distilled water. The solution was dialyzed for 3 days (MWCO 2000 Da), and the resulting solution lyophilized to yield **P3** as a pale yellow solid (559 mg, 45%). SEC: $M_n = 8105$; $M_w = 18\,730$; $M_p = 17\,370$.

Acknowledgment. Financial support from the National Science Foundation under Award No. DMR-9132635 and the NSF-supported MRSEC under Award No. DMR-9632275 is gratefully acknowledged. The authors are grateful to Dr. D-K. Yang for assistance with ^{13}C NMR experiments, Dr. M. Weathers for assistance with powder X-ray diffraction, D. J. Diaz for assistance with AFM, A. Kpissay for help with spin coating, and K. Guthikonda for technical assistance.

References and Notes

(1) (a) Fraser, R. D. B.; MacRae, T. P. *Conformation in Fibrous Proteins and Related Synthetic Polypeptides*; Academic Press: New York, 1973. (b) Urry, D. W. *J. Protein Chem.* **1988**, *7*, 1−34. (c) Perez-Rigueiro, J.; Viney, C.; Llorca, J.; Elices, M. *J. Appl. Polym. Sci.* **2000**, *75*, 1270−1277. (d) For a review, see: Kaplan, D.; Adams, W. W.; Farmer, B.; Viney, C.; Eds. *Silk Polymers: Materials Science and Biotechnology*; ACS Symposium Series 544; American Chemical Society: Washington, DC, 1994.

(2) (a) Rathore, O.; Winningham, M. J.; Sogah, D. Y. *J. Polym. Sci., Part A: Polym. Chem.* **2000**, *38*, 352−366. (b) Winningham, M. J.; Sogah, D. Y. *Macromolecules* **1997**, *30*, 862−876. (c) Sogah, D. Y.; Perle-Treves, D.; Voyer, N.; DeGrado, W. F. *Macromol. Symp.* **1994**, *88*, 149−163.

(3) (a) Sogah, D. Y.; Claussen, R. C.; Winningham, M. J.; Rathore, O. *Annu. Technol. Conf.—Soc. Plast. Eng.* **1999**, 2180−2184. (b) Claussen, R. C.; Sogah, D. Y. *Polym. Prepr. (Am. Chem. Soc., Div. Polym. Chem.)* **1996**, *37*, 394−395. (c) Claussen, R. C. Ph.D. Thesis, Cornell University, 1998.

(4) (a) Qu, Y.; Payne, S. C.; Apkarian, R. P.; Conticello, V. P. *J. Am. Chem. Soc.* **2000**, *122*, 5014. (b) O'Brien, J. P.; Fahnestock, S. R.; Termonia, Y.; Gardner, K. H. *Adv. Mater.* **1998**, *10*, 1185−1195. (c) Fahnestock, S. R.; Bedzyk, L. A. *Appl. Microbiol. Biotechnol.* **1997**, *47*, 33−39. (d) Krejchi, M. T.; Atkins, E. D. T.; Fournier, M. J.; Mason, T. L.; Tirrell, D. A. *J. Macromol. Sci. Pure Appl. Chem.* **1996**, *A33*, 1389−1398. (e) Prince, J. T.; McGrath, K. P.; DiGirolamo, C. M.; Kaplan, D. L. *Biochemistry* **1995**, *34*, 10879−10885. (f) Anderson, J. P.; Cappello, J.; Martin, D. C. *Biopolymers* **1994**, *34*, 1049−1057. (h) Cappello, J.; Crissman, J.; Dorman, M.; Mikolajczak, M.; Textor, G.; Marquet, M.; Ferrari, F. *Biotechnol. Prog.* **1990**, *6*, 198−202.

(5) Titration of **3**, carried out against standardized 0.1 M NaOH solution, revealed an end-group concentration of 2.866 mmol/g.

(6) (a) Nishi, N.; Tsunemi, M.; Hayasaka, H.; Nakajima, B.; Tokura, S. *Makromol. Chem.* **1991**, *192*, 1789−1798. (b) Nishi, N.; Naruse, T.; Hagiwara, K.; Nakajima, B.; Tokura,

S. *Makromol. Chem.* **1991**, *192*, 1799−1809. (c) Nishi, N.; Tsunemi, M.; Nakamura, K.; Tokura, S. *Makromol. Chem.* **1991**, *192*, 1811−1820.
(7) Excess DPPA was added to prevent complications from the presence of TFA.
(8) Miyazawa, T.; Blout, E. R. *J. Am. Chem. Soc.* **1961**, *83*, 712−719.
(9) (a) Wishart, D. S.; Sykes, B. D. *J. Biomol. NMR* **1994**, *4*, 171−80. (b) Saito, H. *Magn. Reson. Chem.* **1986**, *24*, 835−852. (c) Saito, H.; Tabeta, R.; Asakura, T.; Iwanaga, Y.; Shoji, A.; Ozaki, T.; Ando, I. *Macromolecules* **1984**, *17*, 1405−1412.
(10) (a) Seidel, A.; Liivak, O.; Calve, S.; Adaska, J.; Ji, G.; Yang, Z.; Grubb, D.; Zax, D. B.; Jelinski, L. W. *Macromolecules* **2000**, *33*, 775−780. (b) Seidel, A.; Liivak, O.; Jelinski, L. W. *Macromolecules* **1998**, *31*, 6733−6736. (c) Liivak, O.; Blye, A.; Shah, N.; Jelinski, L. W. *Macromolecules* **1998**, *31*, 2947−2951.
(11) (a) Holloway, P. W.; Mantsch, H. H. *Biochemistry* **1989**, *28*, 931−935. (b) Casal, H. L.; Koehler, U.; Mantsch, H. H. *Biochim. Biophys. Acta* **1988**, *957*, 11−20.
(12) (a) Haris, P. I.; Chapman, D. *Biopolymers* **1995**, *37*, 251−263. (b) Torii, H.; Tasumi, M. *J. Chem. Phys.* **1992**, *96*, 3379−3387. (c) Surewicz, W. K.; Mantsch, H. H. *Biochim. Biophys. Acta* **1988**, *952*, 115−130. (d) Bandekar, J.; Krimm, S. *Biopolymers* **1988**, *27*, 885−908. (e) Bandekar, J.; Krimm, S. *Biopolymers* **1988**, *27*, 909−21. (f) Susi, H.; Byler, D. M. *Arch. Biochem. Biophys.* **1987**, *258*, 465−9.
(13) Fraser, R. D. B.; MacRae, T. P.; Stewart, F. H. C.; Suzuki, E. *J. Mol. Biol.* **1965**, *11*, 706−712.
(14) Panitch, A.; Matsuki, K.; Cantor, E. J.; Cooper, S. J.; Atkins, E. D. T.; Fournier, M. J.; Mason, T. L.; Tirrell, D. A. *Macromolecules* **1997**, *30*, 42−49.
(15) Bandrup, J., Immergut, E. H., Eds.; *Polymer Handbook*, 3rd ed.; Wiley-Interscience: New York, 1989.
(16) Chung, L. Z.; Kou, D. L.; Hu, A. T.; Tsai, H. B. *J. Polym. Sci., Part A: Polym. Chem.* **1992**, *30*, 951−953.
(17) (a) Matsen, M. W.; Schick, M. *Macromolecules* **1994**, *27*, 7157−7163. (b) Spontak, R. J.; Smith, S. D.; Ashraf, A. *Macromolecules* **1993**, *26*, 5118−5124. (c) Spontak, R. J.; Zielinski, J. M.; Lipscomb, G. G. *Macromolecules* **1992**, *25*, 6270−6276. (d) Zielinski, J. M.; Spontak, R. J. *Macromolecules* **1992**, *25*, 653−662. (e) Kavassalis, T. A.; Whitmore, M. D. *Macromolecules* **1991**, *24*, 5340−5345. (f) Benoit, H.; Hadziioannou, G. *Macromolecules* **1988**, *21*, 1449−1464. (g) Krause, S. *Macromolecules* **1970**, *3*, 84−86.
(18) (a) Wang, M.; Zhang, L.; Ma, D. *Eur. Polym. J.* **1999**, *35*, 1335−1343. (b) Kajiyama, M.; Kakimoto, M.; Imai, Y. *Macromolecules* **1990**, *23*, 1244−1248. (c) Kajiyama, M.; Kakimoto, M.; Imai, Y. *Macromolecules* **1989**, *22*, 4143−4147. (d) Dwight, D. W.; McGrath, J. E.; Riffle, J. S.; Smith, S. D.; York, G. A. *J. Electron Spectrosc. Relat. Phenom.* **1990**, *52*, 457−473. (e) Patel, N. M.; Dwight, D. W.; Hedrick, J. L.; Webster, D. C.; McGrath, J. E. *Macromolecules* **1988**, *21*, 2689−2696. (f) Nair, C. P. R.; Chaumont, P.; Clouet, G. *J. Macromol. Sci., Chem.* **1990**, *A27*, 791−806. (g) Wlochowicz, A.; Slusarczyk, C.; Strobin, G.; Dems, A. *Angew. Makromol. Chem.* **1988**, *156*, 69−77. (h) Dondero, G.; Pedemonte, E.; Semino, G.; Turturro, A. *Polym. Bull. (Berlin)* **1988**, *19*, 579−585.
(19) (a) Semenov, A. N.; Likhtman, A. E. *Macromolecules* **1998**, *31*, 9058−9071. (b) Semenov, A. N. *J. Phys. II* **1997**, *7*, 1489−1497.
(20) McLean, R. S.; Sauer, B. B. *J. Polym. Sci., Part B: Polym. Phys.* **1999**, *37*, 859−866.
(21) Rodriguez, F. *Principles of Polymer Systems*, 4th ed.; Taylor and Francis: Washington, DC, 1996; pp 696−701.
(22) Trent, J. S. *Macromolecules* **1984**, *17*, 2930−2931.

MA001553X